Catalysis Science & Technology

PAPER

View Article Online
View Journal | View Issue

Cite this: *Catal. Sci. Technol.*, 2017, 7, 293

Water oxidation mediated by ruthenium oxide nanoparticles supported on siliceous mesocellular foam†

Karl P. J. Gustafson,‡[a] Andrey Shatskiy,‡[a] Oscar Verho,§¶[a] Markus D. Kärkäs,||[a] Bastian Schluschass,**[a] Cheuk-Wai Tai,[b] Björn Åkermark,*[a] Jan-Erling Bäckvall*[a] and Eric V. Johnston*[a]

Received 7th October 2016,
Accepted 4th December 2016

DOI: 10.1039/c6cy02121b

www.rsc.org/catalysis

Artificial photosynthesis is an attractive strategy for converting solar energy into fuel. In this context, development of catalysts for oxidation of water to molecular oxygen remains a critical bottleneck. Herein, we describe the preparation of a well-defined nanostructured RuO_2 catalyst, which is able to carry out the oxidation of water both chemically and photochemically. The developed heterogeneous RuO_2 nanocatalyst was found to be highly active, exceeding the performance of most known heterogeneous water oxidation catalysts when driven by chemical or photogenerated oxidants.

Introduction

Today's society is strongly dependent on fossil fuels as the main source of energy. Considering the fact that fossil fuel reserves are being depleted, it is clear that they need to be replaced with sustainable alternatives to ensure the continued growth and development of our society.[1] In order to ascertain a continuous supply of renewable energy that is economically feasible, the raw materials must be abundant and inexpensive. An attractive solution is to use solar energy for production of storable fuels by, *e.g.* splitting of water into molecular oxygen and hydrogen. At present, we do not possess the technology to carry out this intricate process on a commercial scale. One promising approach to achieve this could be to mimic Nature's photosynthetic machinery and employ solar energy for the oxidation of water to molecular oxygen, which can deliver protons and reducing equivalents. In an artificial system, these water-derived reducing equivalents can in turn be utilized to produce the solar fuel of choice. Unfortunately, the design of such artificial photosynthetic systems constitutes a major challenge from an engineering perspective, as it requires the orchestration of several complicated processes, including light absorption, electron transfer from the generated excited state, charge separation, and electron transfer activation of catalysts at physically separated half-reactions. In such artificial schemes, water oxidation (eqn (1)) is considered to be the most critical obstacle since the reaction is highly endergonic and proceeds *via* a highly intricate mechanism. The overall process requires the collective removal of four electrons, coupled with the cleavage of multiple bonds and finally the creation of the O–O bond. These features pose considerable challenges from a chemical perspective and may require interfacing several chemical disciplines in the pursuit of viable water oxidation catalysts (WOCs).[2]

$$2H_2O \rightarrow O_2 + 4H^+ + 4e^- \quad (1)$$

Extensive research during the past decades has therefore focused on the design of robust and efficient WOCs.[3] This has resulted in the construction of a wide array of molecular WOCs based on the metals Ru[4] and Ir,[5] and the more earth-abundant metals Mn,[6] Fe,[7] Co[8] and Cu.[9] However, these molecular WOCs suffer from decomposition and/or deactivation under the highly oxidizing environment required for the water oxidation.[10] An alternative and more attractive approach would be to produce robust heterogeneous catalysts for efficient splitting of water. Since heterogeneous catalysts are not

[a] *Department of Organic Chemistry, Arrhenius Laboratory, Stockholm University, SE-106 91, Stockholm, Sweden. E-mail: bjorn.akermark@su.se, jan.e.backvall@su.se, eric.johnston@su.se*
[b] *Department of Materials and Environmental Chemistry, Arrhenius Laboratory, Stockholm University, SE-106 91, Stockholm, Sweden*

† Electronic supplementary information (ESI) available: Nitrogen absorption/desorption isotherm analysis, XPS spectra, HAADF-STEM characterization of the RuO_2 nanocatalyst, and NMR spectra. See DOI: 10.1039/c6cy02121b

‡ These authors contributed equally.

§ Present address: Center for the Science of Therapeutics, Broad Institute, 415 Main Street, Cambridge, Massachusetts 02142, USA.

¶ Present address: Howard Hughes Medical Institute, Department of Chemistry and Chemical Biology, Harvard University, 12 Oxford Street, Cambridge, Massachusetts 02138, USA.

|| Present address: Department of Chemistry, University of Michigan, Ann Arbor, Michigan 48109, USA.

** Present address: Institut für Anorganische Chemie, Georg-August-Universität, Tammannstraße 4, 37077 Göttingen, Germany.

associated with oxidative degradation to the same extent as their molecular counterparts, they have been extensively studied during the past decades.[11–17] Among these heterogeneous catalysts, nanoparticle-based catalysts have attracted particular attention because of their higher surface-to-volume ratio, which ensures that the majority of the catalytic centers reside on the particle surface and are thus available to participate in catalysis.[18] Today, stabilization of such nanoparticle-based species is possible by immobilization onto, for example, mesoporous materials[19] or metal–organic frameworks (MOFs).[20]

Recently, we reported on a well-characterized heterogeneous catalyst comprised of Pd nanoparticles immobilized on siliceous amino-functionalized mesocellular foam (MCF) for both chemically- and photochemically-induced oxidation of water.[21] Interestingly, this catalyst was found to efficiently catalyze water oxidation at rates comparable to those of state-of-the-art heterogeneous metal-based WOCs,[22,23] while displaying high stability under the reaction conditions employed. In perspective of these results, it was of interest to synthesize and test related Ru-based nanocatalysts given the fact that Ru has proved to be one of the most effective metals for promoting water oxidation.[24–26]

Herein, we report the preparation of a RuO_2 nanocatalyst supported on pyridine-functionalized MCF that is capable of mediating both chemical and photochemical water oxidation. The developed catalyst is a promising candidate for incorporation in a complete photoelectrochemical water splitting cell.[27]

Results and discussion

Synthesis and characterization

It was envisioned that RuO_2 nanoparticles could be firmly anchored to the MCF support surface through a pyridine-based linker. For this purpose, 1-(pyridin-3-yl)-3-(3-(triethoxysilyl)-propyl)urea (PPU) was synthesized as the linker, which can be conveniently grafted onto the MCF through condensation of the alkoxysilane groups of the linker to the silanol groups on the support surface. The synthesis of the RuO_2 nanocatalyst is outlined in Fig. 1 (see Experimental section for further details). Briefly, the PPU linker was synthesized by reacting 3-aminopyridine with triethoxy(3-isocyanatopropyl)-silane in CH_2Cl_2 at room temperature to afford the desired linker in quantitative yield. The MCF material was subsequently grafted with the PPU linker by refluxing a toluene solution of the linker together with MCF for 48 h. The pyridine-functionalized MCF (PPU-MCF) was then impregnated with $RuCl_3$ in water (pH 9) at room temperature to give the Ru^{III}-PPU-MCF precursor. Finally, the MCF-supported Ru^{III} species was reduced by $NaBH_4$, and after exposure to air the RuO_2 nanocatalyst was generated.

The RuO_2 nanocatalyst was characterized by several techniques: N_2 adsorption/desorption measurements, infrared spectroscopy (IR), high-angle annular dark-field scanning transmission electron microscopy (HAADF-STEM), inductively coupled plasma-optical emission spectroscopy (ICP-OES), and X-ray photoelectron spectroscopy (XPS). The anchoring of the linker to the support was confirmed by IR, which showed the presence of a characteristic peak around 1640 cm^{-1} (C═O stretch) belonging to the urea moiety. From ICP-OES analysis, the nitrogen loading of the pristine PPU-MCF support was measured to be 4.55 wt%, which corresponds to a pyridine content of 1.08 mmol g^{-1}. The Ru nanocatalyst was also analyzed by ICP-OES, which measured the Ru and nitrogen loadings to be 7.26 wt% and 2.56 wt%, respectively. Isotherm analysis was conducted on both pristine PPU-MCF and the RuO_2 nanocatalyst (see Table S1†). For the Ru catalyst, the average pore size and window size were determined to be 19.6 nm and 12.4 nm, respectively, and BET surface area analysis

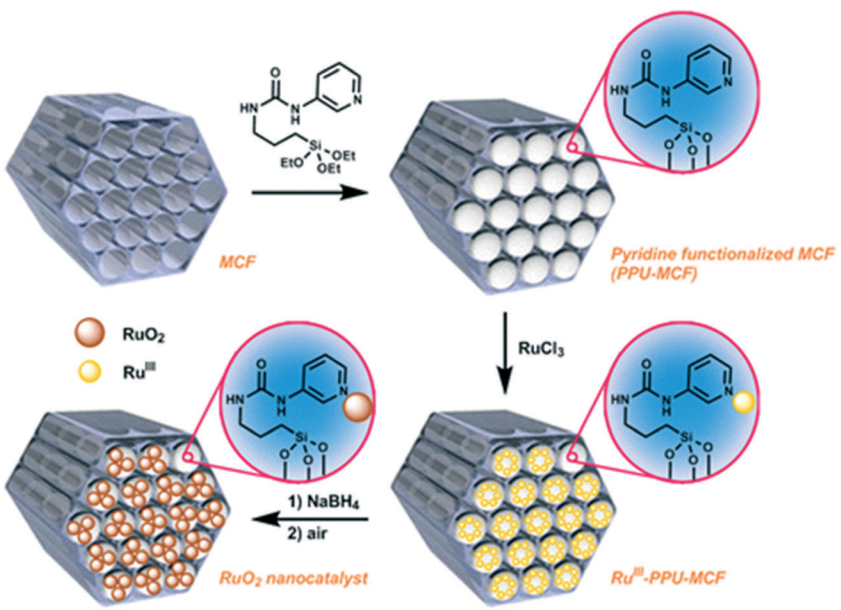

Fig. 1 Synthesis of the RuO_2 nanocatalyst.

showed a specific pore volume and surface area of 1.55 $cm^3\ g^{-1}$ and 341.15 $m^2\ g^{-1}$, respectively. To assess the size and distribution of the RuO_2 nanoparticles, the catalyst was analyzed by HAADF-STEM. This analysis revealed that the catalyst was primarily comprised of subnanometer sized nanoparticles that were well-dispersed on the support surface (Fig. 2). By comparing to previously reported heterogeneous Ru WOCs on mesoporous silica,[24,26] it appears that the extremely small particle size observed for this RuO_2 nanocatalyst is unique and may be promising for achieving high catalytic efficiency. XPS was used to establish the oxidation state of the catalyst. After adjusting the XPS spectrum to the C 1s peak at 285.0 eV as the reference, it was found that the strongest peak of Ru corresponding to the 3d orbital unfortunately overlapped with the 1s signal of C. Therefore the second strongest Ru peak, Ru $3p^{3/2}$, had to be used for determination of the oxidation state. The main Ru $3p^{3/2}$ peak was found at ~463 eV, which is indicative of RuO_2.[28] Oxidation of the reduced catalyst to Ru^{IV} most likely occurs spontaneously once the reduced Ru nanocatalyst is exposed to air, resulting in a more stable RuO_2.

Catalytic activity

The catalytic activity of the developed RuO_2 nanocatalyst was initially evaluated using ceric ammonium nitrate (CAN, Ce^{IV}), which is a strong oxidant that is widely used for screening of WOCs. Upon addition of degassed water to a solid mixture of CAN and the RuO_2 nanocatalyst, O_2 evolution could be observed by real-time mass spectrometry (Fig. 3). Evolution of O_2 was followed for 24 h. The rate of O_2 evolution was found to decrease during the first three hours, after which it became relatively constant. When employing CAN as oxidant, a turnover number (TON; defined as moles of produced O_2 per mole of Ru) of 10 after 24 h and an initial turnover frequency (TOF; defined as moles produced O_2 per mole Ru per unit time) of 24 h^{-1} were obtained for the RuO_2 nanocatalyst.[30]

The catalyst subjected to the abovementioned water oxidation conditions was also recovered and analyzed by XPS, showing an XPS spectrum which is essentially identical to that of the unused catalyst (Fig. S1†). Possible leaching from the catalyst was also tested, but only trace amounts of ruthenium (close to the detection limit, less than 5% of the total amount of used ruthenium) could be observed.

To be practical on the commercial scale, water oxidation ultimately has to be driven by photogenerated oxidants formed by oxidative quenching of the corresponding photosensitizers. Currently, $[Ru(bpy)_3]^{2+}$-complexes (bpy = 2,2′-bipyridine) are the most extensively studied and commonly used photosensitizers for evaluation of WOCs.[31] In this perspective, we were interested to see whether the developed RuO_2 nanocatalyst could promote light-driven water oxidation with a $[Ru(bpy)_3]^{2+}$-type photosensitizer as the light-absorbing component and sodium persulfate ($Na_2S_2O_8$) as the sacrificial electron acceptor. This photodriven system is well-studied[32] and proceeds *via* oxidative quenching of the photoexcited $[Ru(bpy)_3]^{2+*}$ state by $S_2O_8^{2-}$, to generate $[Ru(bpy)_3]^{3+}$, a sulfate ion and a sulfate radical ($SO_4^{\bullet-}$). The chemistry of this system is described in eqn (2)–(4), with the overall reaction shown in eqn (5).

$$[Ru(bpy)_3]^{2+} + h\nu \rightarrow [Ru(bpy)_3]^{2+*} \quad (2)$$

$$[Ru(bpy)_3]^{2+*} + S_2O_8^{2-} \rightarrow [Ru(bpy)_3]^{3+} + SO_4^{\bullet-} + SO_4^{2-} \quad (3)$$

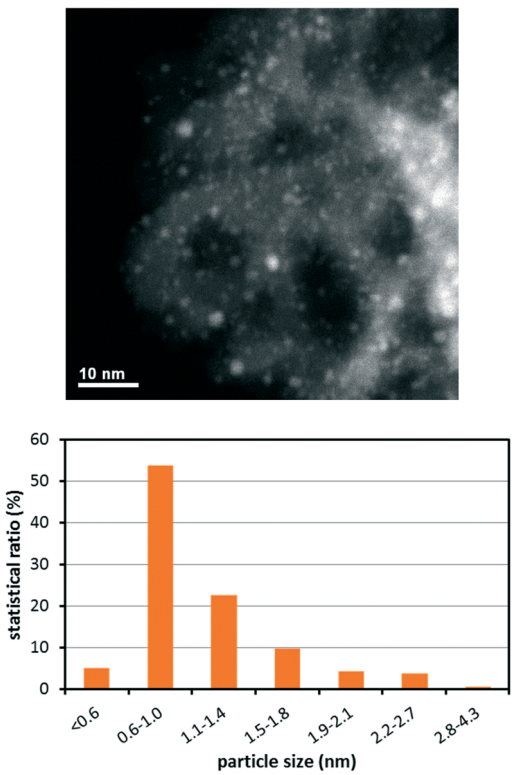

Fig. 2 Structure and particle-size distribution of the RuO_2 nanocatalyst. (Upper) Representative HAADF-STEM image of the RuO_2 nanocatalyst. (Lower) Particle-size distribution for the RuO_2 nanocatalyst with a number-average particle size of 1.1 nm.

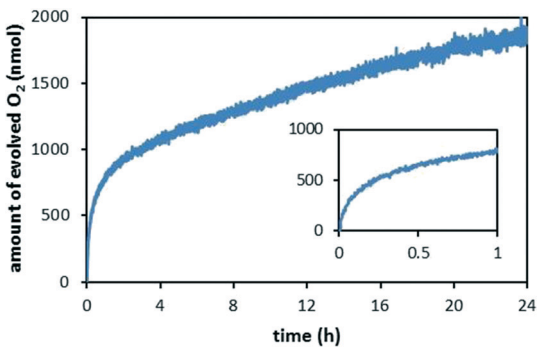

Fig. 3 Background-subtracted O_2 evolution catalyzed by the RuO_2 nanocatalyst using CAN as the chemical oxidant. Conditions: deaerated water (1.0 mL) was added to a solid mixture of RuO_2 nanocatalyst (0.25 mg of the nanocatalyst, containing 0.18 μmol Ru) and CAN (60 mg, 109 μmol). The resulting solution had a pH of ~1.0 (see ref. 29).

$$[Ru(bpy)_3]^{2+} + SO_4^{\bullet -} \rightarrow [Ru(bpy)_3]^{3+} + SO_4^{2-} \quad (4)$$

$$2[Ru(bpy)_3]^{2+} + S_2O_8^{2-} + h\nu \rightarrow 2[Ru(bpy)_3]^{3+} + 2SO_4^{2-} \quad (5)$$

Gratifyingly, when a solution containing the RuO_2 nanocatalyst, persulfate and photosensitizer was irradiated with light (blue LEDs, λ = 420–450 nm), O_2 evolution was triggered and resulted in a TON of 4 with $[Ru(bpy)_3]^{2+}$ as the photosensitizer (Fig. 4). In contrast, control experiments conducted under the same reaction conditions, where either persulfate or light were omitted resulted in negligible oxygen evolution. Moreover, the recovered catalyst displayed an almost unchanged morphology and particle size distribution according to the TEM analysis (Fig. S3 and S4†).[33]

By comparing the catalytic activity of the developed RuO_2 nanocatalyst with other heterogeneous catalysts it is evident that our catalytic system compares well with the current state-of-the-art heterogeneous WOCs (Table 1). Replacing the $[Ru(bpy)_3]^{2+}$ photosensitizer ($E_{1/2}(Ru^{III/II})$ = 1.26 V *vs.* NHE) with $[Ru(bpy)_2(deeb)]^{2+}$ (deeb = diethyl-2,2′-bipyridine-4,4′-dicarboxylate), which has a higher redox potential ($E_{1/2}(Ru^{III/II})$ = 1.40 V *vs.* NHE) resulted in decreased activity and a TON of 1. This trend was observed previously for a related Pd-MCF catalyst;[21] however, the trend is opposite compared to what has been observed for homogeneous WOCs,[4j,6c,36–38] indicating that the decreased activity could be due to the heterogeneous and/or porous nature of the catalyst. It is likely that the more polar carboxy-substituted photosensitizers are strongly absorbed on the MCF walls, precluding diffusion of the photogenerated oxidant to the RuO_2 particles.

Conclusions

Herein, we have reported the synthesis of a heterogeneous catalyst consisting of RuO_2 nanoparticles with an average particle size of 1.1 nm. The catalyst was obtained by immobilizing the Ru nanoparticles on pyridine-functionalized MCF. The synthesized RuO_2 nanocatalyst was evaluated in water oxidation catalysis and was found to mediate both chemical and photochemical water oxidation. In the Ce^{IV}-catalyzed water oxidation, the nanocatalyst reached a TON of 10. Photochemical water oxidation could also be realized, using $[Ru(bpy)_3]^{2+}$-type photosensitizers. The developed nanocatalyst exhibits a higher catalytic performance compared to the majority of the previously reported heterogeneous WOCs. The high activity of the RuO_2 nanocatalyst is ascribed to the high surface-to-volume ratio granted by the small particle size, which makes the majority of the metal centers accessible for catalysis. The results disclosed herein illustrate a non-conventional approach to the design of heterogeneous water oxidation catalysts, where small organic molecules are used to facilitate the synthesis of the supported heterogeneous nanocatalyst. Systematic investigation of the influence of the organic linker on the catalyst structure and performance is currently under investigation.

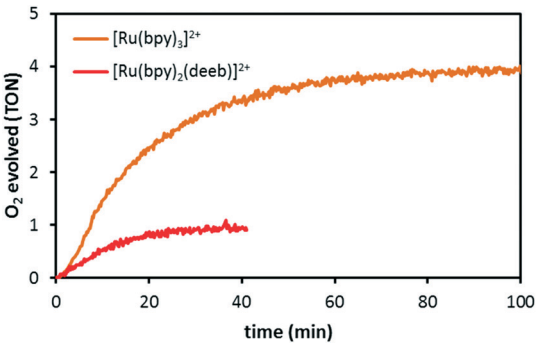

Fig. 4 Photochemical H_2O oxidation catalyzed by the RuO_2 nanocatalyst using $[Ru(bpy)_3](PF_6)_2$ (orange line) and $[Ru(bpy)_2(deeb)](PF_6)_2$ (red line) as photosensitizers. Conditions: an aqueous deaerated phosphate buffer solution (1.0 mL, 0.1 M, pH 7.2) was added to a solid mixture of photosensitizer (5.8 μmol), sodium persulfate (11.6 mg, 49 μmol) and the RuO_2 nanocatalyst (0.50 mg of the nanocatalyst, containing 0.36 μmol Ru).

Table 1 Comparison of water oxidation activity for various heterogeneous catalysts[a]

Catalyst	TON[b]	TOF[c]	Ref.
RuO_2-PPU-MCF	~4.0	2.2×10^{-3} s^{-1}	This work
Pd-MCF	~5.0	2.2×10^{-3} s^{-1}	Ref. 21
RuO_2-SBA-15	~4.0	6.7×10^{-3} s^{-1}	Ref. 34
Mesoporous Mg-Co_3O_4	>0.30	1.6×10^{-4} s^{-1}	Ref. 35
$LaCoO_3$	~0.70	1.4×10^{-3} s^{-1}	Ref. 23
$LiCoMnO_4$	~0.055	8.3×10^{-5} s^{-1}	Ref. 23
$Li_{1.1}Co_2O_4$	~0.10	1.6×10^{-4} s^{-1}	Ref. 23
$Li_2Co_2O_4$	~0.50	9.0×10^{-4} s^{-1}	Ref. 23
$LaMnO_3$	~0.20	4.8×10^{-4} s^{-1}	Ref. 23
Mn_2O_3	~0.23	5.0×10^{-4} s^{-1}	Ref. 23
$MgMn_2O_4$	~0.060	8.2×10^{-5} s^{-1}	Ref. 23

[a] Photochemical oxidation using $[Ru(bpy)_3]^{2+}$ as photosensitizer and $Na_2S_2O_8$ as sacrificial electron acceptor. [b] Turnover number (TON) = amount of evolved O_2/total amount of metal. [c] Turnover frequency (TOF) = turnover per unit time (amount of evolved O_2/{total amount of metal × s}).

Experimental section

Materials and methods

The mesocellular foam (MCF),[39] $[Ru(bpy)_3](PF_6)_2$,[40] and $[Ru(bpy)_2(deeb)](PF_6)_2$ [41] were prepared according to previously reported procedures. All other reagents including solvents were obtained from commercial suppliers and used directly without further purification. All solvents were dried by standard methods when needed. Deionized water was used in all experiments. FTIR spectra were recorded on a Perkin-Elmer Spectrum One spectrometer, using samples prepared as KBr discs.

The physical properties of the mesoporous materials were determined from N_2 adsorption/desorption isotherms using an ASAP 2010 instrument. For TEM analyses, small amounts of grinded RuO_2 nanocatalyst were added to EtOH, ultrasonicated, and a few drops of the resulting slurry were deposited onto a Cu TEM grid with amorphous carbon supporting films (SPI Supplies Inc.). Samples were dried

thoroughly before insertion into the microscope column. For the particle analysis, high-angle annular dark-field scanning transmission electron microscopy (HAADF-STEM) was performed in a 200 kV electron microscope with a Schottky field-emission gun (JEOL JEM-2100). The HAADF-STEM images were recorded using a JEOL ADF detector. The camera length was 8 cm and the incident beam probe size was ~0.2 nm. The gain of the detector was kept constant throughout the experiments of all samples. Since the contrast of RuO_2 in HAADF-STEM images is apparently stronger than that of the MCF support, particle size measurements were possible by careful adjustment of the background threshold. Imaging and particles size analysis were carried out by Gatan Digital Micrograph (Gatan Inc.). X-ray photoelectron spectroscopy (XPS) was used to determine the structure and oxidation states of the Ru nanoparticles on the PPU-MCF material.

Gas analysis by mass spectrometry

Oxygen evolution was measured by MS, where the mass spectrometer consisted of three separate parts connected by gas valves; a reaction chamber, a gas handling system (GHS), and a residual gas analyzer (MKS Spectra Products, Microvision Plus RGA, 0–100 mass units) in ultra-high vacuum (base pressure 2×10^{-10} mbar). A rough pump is used to evacuate the GHS, so the pressure can be regulated within 0.1–1000 mbar. The enclosed volume in the reaction chamber is continuously probed by the mass spectrometer by an inlet through the leak valve. A *ca.* 1 cm thick rubber gasket has been added to the system and permits injection of solutions containing reactants into the reaction chamber, essentially without any leakage of the external atmosphere. Any air leakage is continuously followed by the mass spectrometer (by increase of both O_2 and N_2). In order to avoid splashing when injecting the solution, a pressure of ~40 mbar is needed and in this study the enclosed volume was filled with He to obtain the desired pressure.

The change over time of the measured signal of masses 0–100 in the mass spectrometer is thus converted to the amount in the enclosed volume in two steps. The first step is to convert the signal from the mass spectrometer to pressure in the enclosed volume. This conversion is done by calibration of the system, *i.e.* measuring the response in the MS to different pressures in the enclosed volume. In the second step the pressures in the enclosed volume are converted to the amounts of the different gases by using the gas law, which makes it possible to determine the production of gases with masses 1–100 quantitatively.

Chemical oxidation with Ce^{IV}

In a typical run, the Ru nanocatalyst (0.25 mg RuO_2 nanocatalyst, 7.26 wt% Ru, 0.18 μmol Ru) and $(NH_4)_2[Ce(NO_3)_6]$ (60.0 mg, 0.11 mmol) were placed in the reaction chamber and the reaction chamber was evacuated with a rough pump. ~40 mbar He was then introduced into the system. After an additional 5 min, deoxygenated water (1.0 mL, MilliQ) purged with N_2 for at least 10 min, was injected into the reaction chamber. The generated oxygen gas was then measured and recorded *versus* time by MS.

Photochemical oxidation using $[Ru(bpy)_3]^{2+}$-type photosensitizers

In a typical run, $[Ru(bpy)_3]^{2+}$-type photosensitizer (5.8 μmol), sodium persulfate (11.6 mg, 49 μmol) and Ru nanocatalyst (0.50 mg RuO_2 nanocatalyst, 7.26 wt% Ru, 0.36 μmol Ru) were placed in the reaction chamber. ~40 mbar He was then introduced into the system. After an additional 5 min deoxygenated aqueous phosphate buffer solution (0.1 M, pH 7.2, 1.0 mL) purged with N_2 for at least 10 min, was injected into the reaction chamber and the reaction was irradiated by blue LED light. To avoid heating of the reaction by the light source, the reaction vessel was placed in a water bath and cooled with a small flow of water. The generated oxygen gas was measured and recorded *versus* time by MS.

Procedure for recovering of the RuO_2 nanocatalyst after catalytic water oxidation experiments

After having scaled up the catalytic experiments (×4) with CAN (5 h reaction time), the reaction solution was transferred to a Falcon tube (15 mL), suspended in water (10.0 mL, MilliQ) and centrifuged (4100 rpm, 5 min). The supernatant was removed and the RuO_2 nanocatalyst was resuspended in water (10 mL) and centrifuged (4100 rpm, 5 min). This was repeated 3 times and the resulting solid was dried under vacuum overnight.

Synthesis of 1-(pyridin-3-yl)-3-(3-(triethoxysilyl)propyl)urea (PPU)

3-Aminopyridine (1.90 g, 20.2 mmol) dissolved in CH_2Cl_2 (4.0 mL) was added dropwise to a solution of triethoxy(3-isocyanatopropyl)silane (5.00 g, 20.2 mmol) in CH_2Cl_2 (5.0 mL). The reaction was stirred at room temperature for 48 h. The solution was evaporated to afford the title compound as pale yellow crystals in quantitative yield without the need of any further purification. ^{1}H NMR (400 MHz, $CDCl_3$): δ = 8.32 (m, 1H), 8.18 (m, 1H), 8.03 (m, 1H), 7.90 (s, 1H), 7.19 (m, 1H), 5.62 (m, 1H), 3.79 (q, J = 7.1 Hz, 6H), 3.23 (m, 2H), 1.62 (m, 2H), 1.19 (t, J = 7.1, 9H), 0.63 (m, 2H); ^{13}C NMR (101 MHz, $CDCl_3$): δ = 156.1, 143.5, 140.6, 137.0, 126.8, 124.2, 58.8, 42.9, 23.8, 18.6, 7.9; HRMS (ESI) calcd. for $C_{15}H_{28}N_3O_4SiNa$ $[M + Na^+]^+$: 364.1669; found: 364.1663.

Functionalization of MCF with 1-(pyridin-3-yl)-3-(3-(triethoxysilyl)propyl)urea

MCF (500 mg) and 1-(pyridin-3-yl)-3-(3-(triethoxysilyl)propyl)-urea (PPU, 3.40 g, 9.95 mmol) were placed under vacuum for 1 h. The flask was filled with argon gas upon addition of toluene (12.0 mL) and the reaction mixture was refluxed for 48 h. The reaction was then cooled to room temperature and the solid was washed with toluene (200 mL), CH_2Cl_2 (200 mL) and EtOH (200 mL). The functionalized MCF was resuspended in EtOH and heated overnight at 60 °C, after

which the suspension was filtered and washed with additional EtOH (200 mL) and CH_2Cl_2 (200 mL). The amine loading was determined to be 4.55 wt% using ICP-OES. FTIR λ (cm^{-1}): 3450, 1642, 1557, 1400, 1385, 1088, 802.

Preparation of the RuO_2 nanocatalyst

Functionalized MCF (100 mg) was suspended in pH-adjusted deionized water (7.5 mL, adjusted to pH 9.0 using 0.1 M LiOH) solution in a Falcon tube and stirred for 10 min. $RuCl_3$ (36 mg, 0.175 mmol) was suspended in pH-adjusted deionized water (7.5 mL) and added to the suspension of PPU-MCF. The mixture was stirred at room temperature overnight, deionized water was subsequently added, and the mixture was centrifuged (4100 rpm, 8 min). The dark solid was subsequently washed with water (8 × 45 mL). The solid was resuspended in water (7.5 mL) and reduced by slow addition of a solution of $NaBH_4$ (67.0 mg, 1.77 mmol) in water (2.5 mL), and the mixture was stirred for 30 min. Centrifugation of the mixture was followed by washing of the suspension with water (3 × 45 mL) and acetone (3 × 45 mL). Before use the catalyst was dried under vacuum overnight, and the catalyst was stored under air at room temperature. The amine and ruthenium loadings were determined using ICP-OES to be 2.56 and 7.26 wt%, respectively. FTIR λ (cm^{-1}): 3456, 1640, 1553, 1487, 1401, 1385, 1089, 802.

Acknowledgements

Financial support from the Swedish Research Council (621-2010-4737, 621-2013-4653 and 621-2013-4872), the Berzelii Centre EXSELENT, the European Research Council (ERC AdG 247014), and the Knut and Alice Wallenberg Foundation are gratefully acknowledged.

Notes and references

1 (*a*) H. B. Gray, *Nat. Chem.*, 2009, **1**, 7; (*b*) J. Tollefsson, *Nature*, 2011, **473**, 134–135; (*c*) M. D. Kärkäs, E. V. Johnston, O. Verho and B. Åkermark, *Acc. Chem. Res.*, 2014, **47**, 100–111.

2 (*a*) L. Sun, L. Hammarström, B. Åkermark and S. Styring, *Chem. Soc. Rev.*, 2001, **30**, 36–49; (*b*) J. Barber, *Chem. Soc. Rev.*, 2009, **38**, 185–196.

3 M. D. Kärkäs, O. Verho, E. V. Johnston and B. Åkermark, *Chem. Rev.*, 2014, **114**, 11863–12001.

4 (*a*) H.-W. Tseng, R. Zong, J. T. Muckerman and R. Thummel, *Inorg. Chem.*, 2008, **47**, 11763–11773; (*b*) F. Bozoglian, S. Romain, M. Z. Ertem, T. K. Todorova, C. Sens, J. Mola, M. Rodríguez, I. Romero, J. Benet-Buchholz, X. Fontrodona, C. J. Cramer, L. Gagliardi and A. Llobet, *J. Am. Chem. Soc.*, 2009, **131**, 15176–15187; (*c*) Z. Chen, J. J. Concepcion, X. Hu, W. Yang, P. G. Hoertz and T. J. Meyer, *Proc. Natl. Acad. Sci. U. S. A.*, 2010, **107**, 7225–7229; (*d*) M. D. Kärkäs, T. Åkermark, E. V. Johnston, S. R. Karim, T. M. Laine, B.-L. Lee, T. Åkermark, T. Privalov and B. Åkermark, *Angew. Chem., Int. Ed.*, 2012, **51**, 11589–11593; (*e*) L. Duan, F. Bozoglian, S. Mandal, B. Stewart, T. Privalov, A. Llobet and L. Sun, *Nat. Chem.*, 2012, **4**, 418–423; (*f*) M. R. Norris, J. J. Concepcion, D. P. Harrison, R. A. Binstead, D. L. Ashford, Z. Fang, J. L. Templeton and T. J. Meyer, *J. Am. Chem. Soc.*, 2013, **135**, 2080–2083; (*g*) C. J. Richmond, R. Matheu, A. Poater, L. Falivene, J. Benet-Buchholz, X. Sala, L. Cavallo and A. Llobet, *Chem. – Eur. J.*, 2014, **20**, 17282–17286; (*h*) L. Wang, L. Duan, Y. Wang, M. S. G. Ahlquist and L. Sun, *Chem. Commun.*, 2014, **50**, 12947–12950; (*i*) J. T. Muckerman, M. Kowalczyk, Y. M. Badiei, D. E. Polyansky, J. J. Concepcion, R. Zong, R. P. Thummel and E. Fujita, *Inorg. Chem.*, 2014, **53**, 6904–6913; (*j*) T. M. Laine, M. D. Kärkäs, R.-Z. Liao, T. Åkermark, B.-L. Lee, E. A. Karlsson, P. E. M. Siegbahn and B. Åkermark, *Chem. Commun.*, 2015, **51**, 1862–1865; (*k*) T. M. Laine, M. D. Kärkäs, R.-Z. Liao, P. E. M. Siegbahn and B. Åkermark, *Chem. – Eur. J.*, 2015, **21**, 10039–10048; (*l*) M. D. Kärkäs, R.-Z. Liao, T. M. Laine, T. Åkermark, S. Ghanem, P. E. M. Siegbahn and B. Åkermark, *Catal. Sci. Technol.*, 2016, **6**, 1306–1319.

5 (*a*) N. D. McDaniel, F. J. Coughlin, L. L. Tinker and S. Bernhard, *J. Am. Chem. Soc.*, 2008, **130**, 210–217; (*b*) N. D. Schley, J. D. Blakemore, N. K. Subbaiyan, C. D. Incarvito, F. D'Souza, R. H. Crabtree and G. W. Brudvig, *J. Am. Chem. Soc.*, 2011, **133**, 10473–10481.

6 (*a*) J. Limburg, J. S. Vrettos, L. M. Liable-Sands, A. L. Rheingold, R. H. Crabtree and G. W. Brudvig, *Science*, 1999, **283**, 1524–1527; (*b*) Y. Gao, T. Åkermark, J. Liu, L. Sun and B. Åkermark, *J. Am. Chem. Soc.*, 2009, **131**, 8726–8727; (*c*) E. A. Karlsson, B.-L. Lee, T. Åkermark, E. V. Johnston, M. D. Kärkäs, J. Sun, Ö. Hansson, J.-E. Bäckvall and B. Åkermark, *Angew. Chem., Int. Ed.*, 2011, **50**, 11715–11718; (*d*) E. A. Karlsson, B.-L. Lee, R.-Z. Liao, T. Åkermark, M. D. Kärkäs, V. Saavedra Becerril, P. E. M. Siegbahn, X. Zou, M. Abrahamsson and B. Åkermark, *ChemPlusChem*, 2014, **79**, 936–950; (*e*) W. A. A. Arafa, M. D. Kärkäs, B.-L. Lee, T. Åkermark, R.-Z. Liao, H.-M. Berends, J. Messinger, P. E. M. Siegbahn and B. Åkermark, *Phys. Chem. Chem. Phys.*, 2014, **16**, 11950–11964; (*f*) R.-Z. Liao, M. D. Kärkäs, B.-L. Lee, B. Åkermark and P. E. M. Siegbahn, *Inorg. Chem.*, 2015, **54**, 342–351.

7 (*a*) W. C. Ellis, N. D. McDaniel, S. Bernhard and T. J. Collins, *J. Am. Chem. Soc.*, 2010, **132**, 10990–10991; (*b*) J. L. Fillol, Z. Codolà, I. Garcia-Bosch, L. Gómez, J. J. Pla and M. Costas, *Nat. Chem.*, 2011, **3**, 807–813; (*c*) C. Panda, J. Debgupta, D. Díaz Díaz, K. K. Singh, S. Sen Gupta and B. B. Dhar, *J. Am. Chem. Soc.*, 2014, **136**, 12273–12282; (*d*) M. K. Coggins, M.-T. Zhang, A. K. Vannucci, C. J. Dares and T. J. Meyer, *J. Am. Chem. Soc.*, 2014, **136**, 5531–5534; (*e*) B. Das, A. Orthaber, S. Ott and A. Thapper, *ChemSusChem*, 2016, **9**, 1178–1186; (*f*) B. Das, B.-L. Lee, E. A. Karlsson, T. Åkermark, A. Shatskiy, S. Demeshko, R.-Z. Liao, T. M. Laine, M. Haukka, E. Zeglio, A. F. Abdel-Magied, P. E. M. Siegbahn, F. Meyer, M. D. Kärkäs, E. V. Johnston, E. Nordlander and B. Åkermark, *Dalton Trans.*, 2016, **45**, 13289–13293.

8 (*a*) Q. Yin, J. M. Tan, C. Besson, Y. V. Geletti, D. G. Musaev, A. E. Kuznetsov, Z. Luo, K. I. Hardcastle and C. L. Hill,

Science, 2010, **328**, 342–345; (*b*) D. K. Dogutan, R. McGuire Jr. and D. G. Nocera, *J. Am. Chem. Soc.*, 2011, **133**, 9178–9180; (*c*) X. Zhou, F. Li, H. Li, B. Zhang, F. Yu and L. Sun, *ChemSusChem*, 2014, **7**, 2453–2456; (*d*) M. Chen, S.-M. Ng, S.-M. Yiu, K.-C. Lau, R. J. Zeng and T.-C. Lau, *Chem. Commun.*, 2014, **50**, 14956–14959; (*e*) D. W. Crandell, S. Ghosh, C. P. Berlinguette and M.-H. Baik, *ChemSusChem*, 2015, **8**, 844–852; (*f*) B. Das, A. Orthaber, S. Ott and A. Thapper, *Chem. Commun.*, 2015, **51**, 13074–13077.

9 (*a*) S. M. Barnett, K. I. Goldberg and J. M. Mayer, *Nat. Chem.*, 2012, **4**, 498–502; (*b*) Z. Chen and T. J. Meyer, *Angew. Chem., Int. Ed.*, 2013, **52**, 700–703; (*c*) M. K. Coggins, M.-T. Zhang, Z. Chen, N. Song and T. J. Meyer, *Angew. Chem., Int. Ed.*, 2014, **53**, 12226–12230; (*d*) X.-J. Su, M. Gao, L. Jiao, R.-Z. Liao, P. E. M. Siegbahn, J.-P. Cheng and M.-T. Zhang, *Angew. Chem., Int. Ed.*, 2015, **54**, 4909–4914.

10 (*a*) J. D. Blakemore, N. D. Schley, G. W. Olack, C. D. Incarvito, G. W. Brudvig and R. H. Crabtree, *Chem. Sci.*, 2011, **2**, 94–98; (*b*) M. D. Kärkäs, T. Åkermark, H. Chen, J. Sun and B. Åkermark, *Angew. Chem., Int. Ed.*, 2013, **52**, 4189–4193.

11 J. R. Galán-Mascarós, *ChemElectroChem*, 2015, **2**, 37–50.

12 C.-H. Kuo, I. M. Mosa, A. S. Poyraz, S. Biswas, A. M. El-Sawy, W. Song, Z. Luo, S.-Y. Chen, J. F. Rusling, J. He and S. L. Suib, *ACS Catal.*, 2015, **5**, 1693–1699.

13 C. C. L. McCrory, S. Jung, I. M. Ferrer, S. M. Chatman, J. C. Peters and T. F. Jaramillo, *J. Am. Chem. Soc.*, 2015, **137**, 4347–4357.

14 X. Lu and C. Zhao, *Nat. Commun.*, 2015, **6**, 6616.

15 H. S. Ahn, J. Yano and T. D. Tilley, *ACS Catal.*, 2015, **5**, 2573–2576.

16 H. N. Nong, H.-S. Oh, T. Reier, E. Willinger, M.-G. Willinger, V. Petkov, D. Teschner and P. Strasser, *Angew. Chem., Int. Ed.*, 2015, **54**, 2975–2979.

17 Y. Hou, Z. Wen, S. Cui, S. Ci, S. Mao and J. Chen, *Adv. Funct. Mater.*, 2015, **25**, 872–882.

18 K. An and G. A. Somorjai, *ChemCatChem*, 2012, **4**, 1512–1524.

19 (*a*) V. Malgras, Q. Ji, Y. Kamachi, T. Mori, F.-K. Shieh, K. C.-W. Wu, K. Ariga and Y. Yamauchi, *Bull. Chem. Soc. Jpn.*, 2015, **88**, 1171–1200; (*b*) N. L. Torad, Y. Li, S. Ishihara, K. Ariga, Y. Kamachi, H.-Y. Lian, H. Hamoudi, Y. Sakka, W. Chaikittisilp, K. C.-W. Wu and Y. Yamauchi, *Chem. Lett.*, 2014, **43**, 717–719; (*c*) K. C.-W. Wuab and Y. Yamauchi, *J. Mater. Chem.*, 2012, **22**, 1251–1256.

20 H.-W. Chen, Y.-D. Chiang, C.-W. Kung, N. Sakai, M. Ikegami, Y. Yamauchi, K. C.-W. Wu, T. Miyasaka and K.-C. Ho, *J. Power Sources*, 2014, **245**, 411–417.

21 O. Verho, T. Åkermark, E. V. Johnston, K. P. J. Gustafsson, C.-W. Tai, H. Svengren, M. D. Kärkäs, J.-E. Bäckvall and B. Åkermark, *Chem. – Eur. J.*, 2015, **21**, 5909–5915.

22 A. Mills, P. A. Duckmanton and J. Reglinski, *Chem. Commun.*, 2010, **46**, 2397–2398.

23 U. Maitra, B. S. Naidu, A. Govindaraj and C. N. R. Rao, *Proc. Natl. Acad. Sci. U. S. A.*, 2013, **110**, 11704–11707.

24 Y. Zhang, E. C. Judkins, D. R. McMillin, D. Mehta and T. Ren, *ACS Catal.*, 2013, **3**, 2474–2478.

25 Y. Zhang and T. Ren, *Chem. Commun.*, 2012, **48**, 11005–11007.

26 N. C. King, C. Dickinson, W. Zhou and D. W. Bruce, *Dalton Trans.*, 2005, 1027–1032.

27 D. M. Fabian, S. Hu, N. Singh, F. A. Houle, T. Hisatomi, K. Domen, F. E. Osterloh and S. Ardo, *Energy Environ. Sci.*, 2015, **8**, 2825–2850.

28 C. D. Wagner, W. M. Riggs, L. E. Davis, J. F. Moulder and G. E. Muilenberg, *Handbook of X-ray Photoelectron Spectroscopy*, Physical Electronics Division, Perkin-Elmer, Eden Prairie, MN, 1979, vol. 55, p. 344.

29 S. A. Hayes, P. Yu, T. J. O'Keefe, M. J. O'Keefe and J. O. Stoffer, *J. Electrochem. Soc.*, 2002, **149**, C623–C630.

30 A "steady-state" TOF of 0.33 h^{-1} was obtained over a 24 h reaction time.

31 A. Juris, V. Balzani, F. Barigelletti, S. Campagna, P. Belser and A. von Zelewsky, *Coord. Chem. Rev.*, 1988, **84**, 85–277.

32 F. Bolletta, A. Juris, M. Maestri and D. Sandrini, *Inorg. Chim. Acta*, 1980, **44**, L175–L176.

33 The leaching and XPS analysis were prohibited due to inevitable deposition of the ruthenium photosensitizer on the catalyst, rendering the results inconclusive.

34 Y. Zhang, E. C. Judkins, D. R. McMillin, D. Mehta and T. Ren, *ACS Catal.*, 2013, **3**, 2474–2478.

35 J. Rosen, G. S. Hutchings and F. Jiao, *J. Am. Chem. Soc.*, 2013, **135**, 4516–4521.

36 M. D. Kärkäs, E. V. Johnston, E. A. Karlsson, B.-L. Lee, T. Åkermark, M. Shariatgorji, L. Ilag, Ö. Hansson, J.-E. Bäckvall and B. Åkermark, *Chem. – Eur. J.*, 2011, **17**, 7953–7959.

37 Y. Xu, L. Duan, L. Tong, B. Åkermark and L. Sun, *Chem. Commun.*, 2010, **46**, 6506–6508.

38 Y. Xu, A. Fischer, L. Duan, L. Tong, E. Gabrielsson, B. Åkermark and L. Sun, *Angew. Chem., Int. Ed.*, 2010, **49**, 8934–8937.

39 M. M. Taqui Khan, R. C. Bhardwaj and C. Bhardwaj, *Polyhedron*, 1990, **9**, 1243–1248.

40 H. Xia, Y. Zhu, D. Lu, M. Li, C. Zhang, B. Yang and Y. Ma, *J. Phys. Chem. B*, 2006, **110**, 18718–18723.

41 R. E. DeSimone and R. S. Drago, *J. Am. Chem. Soc.*, 1970, **92**, 2343–2352.